AGU Advances

RESEARCH ARTICLE
10.1029/2021AV000396

Recent Warming Fuels Increased Organic Carbon Export From Arctic Permafrost

Xiaowen Zhang[1,2,3], Thomas S. Bianchi[1], Andrea J. M. Hanna[4], Michael R. Shields[1,5], Gareth Izon[3], Jack A. Hutchings[6], Chien-Lu Ping[7], Mikhail Kanevskiy[8], Negar Haghipour[9,10], and Timothy I. Eglinton[9]

[1]Department of Geological Sciences, University of Florida, Gainesville, FL, USA, [2]School of Oceanography, Shanghai Jiao Tong University, Shanghai, China, [3]Department of Earth, Atmospheric and Planetary Sciences, Massachusetts Institute of Technology, Cambridge, MA, USA, [4]Jackson School of Geosciences, Institute of Geophysics, University of Texas at Austin, Austin, TX, USA, [5]Geochemical and Environmental Research Group, Texas A&M University, College Station, TX, USA, [6]Department of Earth and Planetary Sciences, Washington University, St. Louis, MO, USA, [7]School of Natural Resources and Extension, University of Alaska Fairbanks, Fairbanks, AK, USA, [8]Institute of Northern Engineering, University of Alaska Fairbanks, Fairbanks, AK, USA, [9]Department of Earth Sciences, Geological Institute, ETH Zürich, Zürich, Switzerland, [10]Department of Physics, Laboratory of Ion Beam Physics, ETH Zürich, Zürich, Switzerland

Abstract Climate-driven thawing of Arctic permafrost renders its vast carbon reserves susceptible to microbial degradation, serving as a potentially potent positive feedback hidden within the climate system. While seemingly intuitive, the relationship between thermally driven permafrost losses and organic carbon (OC) export remains largely unexplored in natural settings. Filling this knowledge gap, we present down-core bulk and compound-specific radiocarbon records of permafrost change from a sediment core taken within the Alaskan Colville River delta spanning the last *c*. 2,700 years. Fingerprinted by significantly older radiocarbon ages of bulk OC and long-chain fatty acids, these data expose a thermally driven increase in permafrost OC export and/or deepening of mobilizable permafrost layers over the last *c*. 160 years after the Little Ice Age. Comparison of OC content and radiocarbon data between recent and Roman warming episodes likely implies that the rate of warming, alongside the prevailing boundary conditions, may dictate the ultimate fate of the Arctic's permafrost inventory. Our findings highlight the importance of leveraging geological records as archives of Arctic permafrost mobilization dynamics with temperature change.

Plain Language Summary Temperature rise in the Arctic is likely causing enhanced thawing of perennially frozen soil (permafrost), leading to potential decomposition of organic matter and release of greenhouse gases. Models forecasting the potential release of permafrost organic carbon (OC) largely rely on historical records or experimental results over the past decades, leaving large uncertainties for long-term predictions. In this study, a sediment core from the Alaskan Colville River delta was analyzed to provide a sub-centennial long-term record of changes of permafrost OC export. The radiocarbon results of bulk OC demonstrated a close association with temperature change, highlighting the increase of permafrost OC export and/or deepening of mobilizable permafrost layers for the past 160 years as a result of Arctic warming. The 2,700-year record also implies that some factors like the rate of warming and the temperature before warming may need to be considered in climate models for better predictions.

Key Points:

- Arctic warming has likely caused an increase of permafrost organic carbon export and/or deepening of mobilizable permafrost layers over the last 160 years
- Bank erosion is likely a key mechanism of mobilizing permafrost to the coast under warming conditions
- The rate of warming and the prevailing boundary conditions may be important modulators of permafrost thawing

Supporting Information:

Supporting Information may be found in the online version of this article.

Correspondence to:

X. Zhang,
xiaowenz@sjtu.edu.cn

Citation:

Zhang, X., Bianchi, T. S., Hanna, A. J. M., Shields, M. R., Izon, G., Hutchings, J. A., et al. (2021). Recent warming fuels increased organic carbon export from Arctic permafrost. *AGU Advances*, *2*, e2021AV000396. https://doi.org/10.1029/2021AV000396

Received 21 JAN 2021
Accepted 5 APR 2021

Author Contributions:

Conceptualization: Xiaowen Zhang, Thomas S. Bianchi
Formal analysis: Xiaowen Zhang, Andrea J. M. Hanna, Jack A. Hutchings, Negar Haghipour
Funding acquisition: Xiaowen Zhang, Thomas S. Bianchi, Timothy I. Eglinton
Methodology: Xiaowen Zhang, Andrea J. M. Hanna, Michael R. Shields, Negar Haghipour
Resources: Thomas S. Bianchi, Chien-Lu Ping, Mikhail Kanevskiy
Supervision: Thomas S. Bianchi

1. Introduction

Global warming is responsible for dramatic physiogeographic and ecological changes within the Arctic Circle (Elmendorf et al., 2012; Hinzman et al., 2005; Liljedahl et al., 2016; Tape et al., 2006). For example, thermokarst and thermal erosion alter organic carbon (OC) mobilization pathways and impact carbon cycling (McGuire et al., 2009; Schuur et al., 2015). Frozen soils, or permafrost, house *c*. 1,300–1,600 Pg of OC (Schuur et al., 2015) which, upon warming, becomes susceptible to microbial degradation, fostering the release of potent greenhouse gases (i.e., CO_2 and CH_4) (Schuur et al., 2008; Vonk et al., 2012). Therefore, permafrost thawing is anticipated to act as a positive feedback within the climate system, capable of exacerbating climate warming through the destabilization of a long-standing carbon pool (Koven et al., 2011; Schuur et al., 2015).

Writing – original draft: Xiaowen Zhang
Writing – review & editing: Xiaowen Zhang, Thomas S. Bianchi, Andrea J. M. Hanna, Michael R. Shields, Gareth Izon, Jack A. Hutchings, Chien-Lu Ping, Mikhail Kanevskiy, Negar Haghipour, Timothy I. Eglinton

Figure 1. (a) Map depicting the state and extent of permafrost, while locating the (b–c) study area and sampling sites in northern Alaska, USA. Within inset a, continuous (dark purple), discontinuous (purple), and sporadic/isolated permafrost (light purple) are differentiated by color (Brown et al., 1997). Here, the Colville River watershed is outlined in orange in panel (a) and blue in panel (b). Filled black circles depict sampling locations within the (b) Colville River watershed and (c) delta. Maps were created using ArcGIS 10.6 with world ocean basemap.

Currently, ecosystem and Earth system models incorporating permafrost carbon dynamics are principally informed by a combination of historical temperature records, in vitro and laboratory soil respiration experiments and observations of geomorphological change (Koven et al., 2011; Schädel et al., 2016; Smith et al., 2005). While valid, these observational approaches are restricted to the last few decades, which, in turn, precludes the rigorous evaluation of long-term simulations and, indeed, the identification of potential non-linearity within the climate system. To overcome this shortcoming, and to further our understanding of thermally modulated long-term permafrost carbon dynamics, high-resolution sub-centennial records remain paramount. While, in principle, deltaic sedimentary secessions offer integrated centennial to millennial-scale records of watershed-housed carbon cycling (Bianchi & Allison, 2009), within the Arctic, strong coastal currents and intense ice processing (e.g., ice gauging and strudel scour) often compromise their integrity and, where available (Tesi et al., 2016; Winterfeld et al., 2018), the sedimentary records often lack the resolution necessary to reveal high-amplitude dynamics.

To this end, the Colville River Delta, located on the northern coast of Alaska, provides a somewhat unique sedimentary archive; shielded from destructive cryospheric processes (e.g., ice gauging and strudel scour) by barrier islands, the delta features a well-laminated sedimentary record dominated by riverine OC inputs (Hanna et al., 2014; Schreiner et al., 2013; Zhang et al., 2015). Accordingly, to reconstruct northern Alaskan permafrost erosion over the last *c.* 2,700 years, we report radiocarbon ages of bulk OC from a sediment core (L1) collected from the Colville River Delta (Figure 1). Augmenting this record, targeting selected samples, we also conducted complementary radiocarbon analysis of long-chain fatty acids (LCFAs), which as major components in vascular plant leaf wax lipids (Bianchi & Canuel, 2011), serve as an age-resolved biomarker capable of tracing terrestrially derived OC through the Colville watershed. Radiocarbon ages of bulk OC from selected surface soil and upper permafrost samples from the Colville River watershed were

also measured (Figure 1). While clearly not exhaustive in their geographic reach, these soil analyses provide a preliminary context for the likely range of permafrost ages that are present in the Colville River watershed, a region from which very few ^{14}C measurements exist.

2. Materials and Methods

2.1. Study Area and Sampling Strategy

The Colville River originates on the northern slopes of Brooks Range, flowing north through the Arctic Foothills and Coastal Plain, terminating via a delta on the inner shelf of the Beaufort Sea (Figure 1). The watershed is underlain by continuous permafrost. Dwarf shrub coverage typifies the vegetation in the river's upper course, transitioning to greater moss cover toward its terminus (Walker et al., 2005). Like most Arctic catchments, ice break-up and snowmelt discharge occur in late May to early June, promoting an intense flood pulse with riverine discharge reaching up to 6,000 $m^3 s^{-1}$ (Walker & Hudson, 2003). Although oil exploration activities have expanded in the watershed since 2001, particularly at and around the delta, the construction of pipeline, gravel pads, and roads that can potentially trigger thermokarst and thermal erosion are confined in very small zones near those infrastructures (Raynolds et al., 2014). The short-term oil development recorded in our core (2001–2010) is unlikely to have significantly influenced sediment dynamics, especially when contextualized in terms of the seasonal bank erosion associated with the spring freshet (Walker & Hudson, 2003). In addition, minimal oil contamination has been found in nearshore sediments in this region (Venkatesan et al., 2013). More generally, human activity within the watershed is nominal representing a rare and relatively pristine region from which to reconstruct permafrost dynamics.

Simpson Lagoon, adjacent to the Colville River Delta, represents an attractive shallow water (<2.5 m) depocenter archiving Colville River sediments (Dunton et al., 2006; Hanna et al., 2014). Within the lagoon, sediment core L1 was collected in August 2010, using a Rossfelder P-3 submersible vibra corer abroad the *R/V Annika Marie*. After recovery, the core was split lengthwise, sectioned at 2 cm intervals and freeze-dried before analysis. Complementing core L1, selected soil samples were also analyzed in an attempt to, at least partially, represent the age profile for surface and upper permafrost in the wider Colville River watershed. Specifically, soils from Ivotuk and DUM were collected from the upper watershed in 1999 (Michaelson & Ping, 2003) and 2009, which were augmented with additional samples from Itkillik in 2011 (Kanevskiy et al., 2016). Samples from the first two sampling campaigns were air-dried at room temperature, while those from Itkillik were oven-dried at 90°C. While, hypothetically, these treatments could differentially lose volatile organic constituents, researches have estimated the loss to be less than 1% (Schumacher, 2002) and ramped-pyrolysis experiments verified that little CO_2 is lost at temperature below 90°C (Rosenheim & Galy, 2012; Vetter et al., 2017; Zhang et al., 2017), effectively minimizing preparative artifacts and bolstering the bulk OC comparison here.

2.2. Age Model

The age-depth model for core L1 is derived from ^{137}Cs sediment ages and radiocarbon dating of benthic foraminifera (Figure S1). The age model and its uncertainty were determined using the R package BACON (Blaauw & Christen, 2011), which is a Bayesian technique for calibration and age modeling that relies on the Marine 13 radiocarbon calibration curve.

After wet sieving, ^{137}Cs dating was performed on the sub-32 μm sediment fraction. Here, after homogenization, the samples were packed and sealed in 39 mm vials for analysis. Samples were counted for *c.* 48 h on a Canberra low-energy germanium gamma spectrometer after at least 21 days of equilibration. Activities of ^{137}Cs were determined from the 661.6 keV photopeak. The ^{137}Cs activity profile of L1 is demonstrated in Figure 2 from Hanna et al. (2014; named differently as core SL2) and Figure S2, showing a steady-state accumulation of sediments. The reliability of sedimentation rates calculated by ^{137}Cs analysis was verified by $^{239,240}Pu$ analysis of other sediment cores in Simpson Lagoon (Hanna et al., 2014).

Benthic foraminifera (*Elphidium sp.* and *Buccella frigida*) were picked using a binocular microscope. The isolated foraminifera were rinsed and sonicated with DI water and methanol and sent to National Ocean

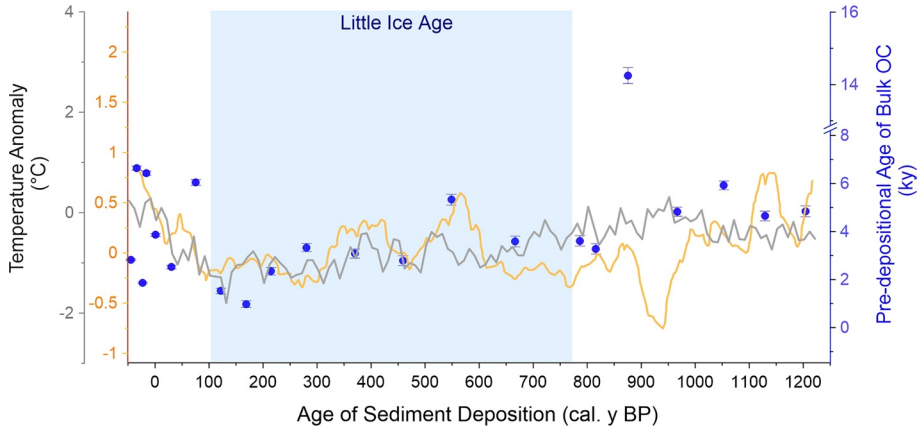

Figure 2. Comparison of pre-depositional ^{14}C ages of bulk OC from Colville River deltaic sediments (blue points) with the PAGES Arctic 2k annual temperature reconstruction (gray line; McKay & Kaufman, 2014) and Brooks Range temperature reconstruction from Blue Lake (orange line; Bird et al., 2009) spanning the last 1,300 years. The blue column highlights the Little Ice Age.

Sciences Accelerator Mass Spectrometry (NOSAMS) facility at the Woods Hole Oceanographic Institution for radiocarbon dating. Reservoir ages were calculated via subtraction of the extrapolated ^{137}Cs age from radiocarbon age directly beneath the first appearance of ^{137}Cs (Hanna et al., 2014).

As shown in Figure S1, the employed BACON approach incorporated both ^{137}Cs and ^{14}C age constraints, culminating an integrated age model. As is common when comparing sedimentation rates over different timescales (Baskaran et al., 2017; Davies et al., 2018), the upper 50 cm of core accumulated faster than its remainder: a feature driven by time-averaging of stratigraphic hiatuses combined with the evolution of fluvial load and oceanographic conditions (Miller & Kuehl, 2010). Nevertheless, as the depositional ages obtained from the two dating methods for upper samples are much younger than the actual ^{14}C ages of bulk OC and LCFAs (Tables S1, S2), the impact on the pre-depositional ages is limited.

2.3. Bulk TOC and $\delta^{13}C$ Analysis

Aliquots (*c.* 5–40 mg) of homogenized sample powders were weighed into silver capsules and decarbonated via HCl fumigation (Harris et al., 2001). After drying at 60°C for 24 h, the capsules were encapsulated in tin and their total organic carbon (TOC) and stable carbon isotope ($\delta^{13}C$) values were determined via flash combustion using a Carlo Erba (NA1500 CNS) elemental analyzer interfaced with a Thermo Delta V Advantage isotope ratio mass spectrometer. Because of the wide range of soil and sediment TOC content, coefficient of variation was used to demonstrate the quality control on TOC measurement, which is within 3.0% for replicate measurements of selected samples. The standard deviation of $\delta^{13}C$ data are within 0.1‰ for replicate measurements of selected samples.

2.4. Isolation of Long-Chain Fatty Acids

Lipids were extracted in dichloromethane:methanol (9:1, v/v) via accelerated solvent extraction and saponified with 15 mL 0.5M KOH in pure methanol and ~150 μL Milli-Q water for 2 h (70°C). After hexane extraction of the neutral fraction, the remaining aqueous solution was acidified and extracted with hexane:dichloromethane (4:1, v/v). The acidic fraction was evaporated to incipient dryness and derivatized with methanoic BF_3 to form fatty acid methyl esters (FAMEs). FAMEs were purified initially via elution with dichloromethane from a 2 cm silica gel column. Following a second silica gel column-pass, the purified FAMEs were collected in hexane:dicholoromethane (1:1, v/v) subsequent to matrix elution in hexane. The hexane:dicholoromethane fraction was used for collecting individual long-chain FAME on a preparative capillary gas chromatograph (PC-GC) (Eglinton et al., 1996). Given their comparable ^{14}C ages (Feng et al., 2015), C_{24}, C_{26}, C_{28}, C_{30}, and C_{32} fatty acids were ultimately combined for radiocarbon analysis. The

purity of the combined FAME mixtures was verified by elution from a silica gel column and subsequent GC-FID analysis.

2.5. Radiocarbon Analysis of Bulk OC and LCFAs

Aliquots of carbonate-free sediments and purified FAME fractions were graphitized at the University of Florida and measured at NOSAMS facility, Woods Hole Oceanographic Institution. Here, upon sealing under vacuum in quartz tubes, carbon was oxidized to CO_2 in the presence of CuO at 900°C for 3 h. The resultant gas was then cryogenically purified before isolation in Pyrex® reactor tubes and was converted to graphite via zinc reduction (Xu et al., 2007) with sequential combustion at 500°C for 3 h and 550°C for 4 h. Radiocarbon ages of bulk OC and LCFAs were corrected for preparative and instrumentally introduced biases using primary standard (oxalic acid 4990C), secondary standard oxalic acid C7 and coal blanks, assuming constant contamination introduced during GC collection and on vacuum line (Haghipour et al., 2018).

The remaining bulk sediments and FAME fractions were converted to CO_2 via combustion using an elemental analyzer (EA) interfaced with a Mini carbon dating system (MICADAS) at the accelerator mass spectrometry (AMS) facility at ETH, Zurich. In detail, bulk sediments were first decarbonated via a 72 h fumigation with 37% HCl (TM grade) at 70°C. Carbonate-free residues were neutralized with NaOH, dried and combusted in tin capsule where the product CO_2 was measured by EA-AMS. Naturally, the decarbonation process was not necessary for the purified FAME fractions, which were immediately transferred to liquid-specific capsules using dichloromethane:hexane (1:1, v:v) and analyzed by EA-AMS. Samples were normalized using oxalic acid II (NISTSRM4990C) and corrected for constant contamination introduced during fumigation and combustion (Haghipour et al., 2018).

For the LCFAs, the blank contribution associated with PC-GC FAME collection was obtained by identical treatment of a ^{14}C-dead C_{28} alkane (O-504, Sigma-Aldrich) and a ^{14}C-modern C_{32} alkane (D223107, Sigma-Aldrich) standard. These standards were collected via PC-GC preparation after 40 and 80 injections, demonstrating the procedurally induced addition of 1.9 ± 0.38 μg of C with a fraction modern (Fm) of 0.68 ± 0.21. The ^{14}C ages of FAMEs were then corrected for the addition of a radiocarbon-dead methyl group during derivatization to obtain mean ^{14}C age of LCFAs

$$\mathrm{Fm}_{\mathrm{LCFA}} = \mathrm{Fm}_{\mathrm{FAME}} \times n_c \,/\, \left(n_c - 1\right)$$

where $\mathrm{Fm}_{\mathrm{LCFA}}$ is the final fraction modern of fatty acids, $\mathrm{Fm}_{\mathrm{FAME}}$ is the fraction modern for FAMEs after correction for instrumental contamination and n_c is the weighted average carbon number in the FAME mixture:

$$n_c = \left(f_{c25} \times 25 + f_{c27} \times 27 + f_{c29} \times 29 + f_{c31} \times 31 + f_{c33} \times 33\right)$$

where f_{c25}, f_{c27}, f_{c29}, f_{c31}, and f_{c33} are the relative proportions of FAMEs in a given mixture, corresponding to C_{24}, C_{26}, C_{28}, C_{30}, and C_{32} fatty acids.

2.6. Calculation of Pre-Depositional Age and Its Significance

The calibrated sample age (X) describes the ^{14}C age of a given sample after correction for preparative and instrumentally induced biases, while the calibrated depositional age (Y) is the age obtained from age model. The difference between these ages yields the pre-depositional age (i.e., $Z = X - Y$). The uncertainty (σ_Z) associated with the pre-depositional age (Z), therefore, propagates from those associated with X and Y, summing in quadrature to give: $\sigma_Z = \sqrt{(\sigma_X^2 + \sigma_Y^2)}$. For LCFAs, pre-depositional mean age was used as the ^{14}C composition actually reflects the weighted mean of the mixed fatty acids inventory of a given sample (Eglinton et al., 2021).

2.7. Statistical Analysis

We compared the pre-depositional mean ^{14}C ages of LCFAs of sediment samples using a *t*-test, a Wilcoxon rank sum test, and a Monte Carlo balanced bootstrap approach in R program. For Monte Carlo balanced bootstrap approach, the pre-depositional mean LCFAs ages and their associated uncertainties (σ_Z) were used to generate a normal distribution of 10^6 for each sample using *rnorm* function. These distributions were then sampled without replacement and subsampled into 10^6 bootstrap replicates with the intention of matching the original sample structure of the LCFAs data.

3. Results

The down-core stable carbon isotope ($\delta^{13}C$) record of bulk OC is relatively invariant over the past *c.* 2,700 years, with an average $\delta^{13}C$ value of -26.5 ± 0.2‰ (1 S.D, Table S1). Contrasting with ^{13}C-enriched marine inputs, this average $\delta^{13}C$ value is nearly identical to that of the fluvial deposits near the river mouth (−26.6‰) which most likely reflect sediments delivered during the spring freshet (Feng et al., 2015), implying the dominance of riverine inputs at this site. This agrees with the terrestrial biomarker results from the upper 50 cm of L1 (Zhang et al., 2015) and modeled dominance of OC sourced from the Colville River in L1 surface sediments (83%; Schreiner et al., 2013). The pre-depositional ^{14}C ages of bulk OC range from 977 to 14,248 years, either are younger than, or approximate, the bulk ^{14}C ages of the soil samples analyzed from the Colville River watershed (Table S2). Considering the dilution effect of OC from fresh surface soils and minor marine inputs on the bulk ^{14}C ages, these pre-depositional ^{14}C ages of bulk OC imply continuous permafrost OC inputs to the delta.

Over the past *c.* 2,700 years, the pre-depositional ^{14}C ages of bulk OC show moderate variability, with a pronounced outlier deposited at *c.* 900 cal. y BP (Figure 2; Table S2). Given that the OC at this depth is much older than the enveloping sediment and, indeed, the record as a whole, we suggest that this sample records an interesting but apparently atypical event that resulted in the significant addition of pre-aged carbon to the study site. Excluding this outlier, the pre-depositional ^{14}C age of bulk OC defines a gradual decreasing trend that parallels the long-term cooling trend seen between *c.* 1,200 cal. y BP and *c.* 100 cal. y BP (Figure 2). Based on the temperature reconstructions in central Brooks Range and the Arctic (Figure 2), *c.* 100 cal. y BP marks the termination of the Little Ice Age (LIA), beyond which the pre-depositional ^{14}C ages of bulk OC show an apparent increase that parallels the abrupt temperature rise seen over the past *c.* 160 years. The youngest pre-depositional ^{14}C age of bulk OC (977 ± 142 years; Figure 2) was observed near the end of LIA. Subsequent warming coincides with highly variable but generally older pre-depositional ^{14}C ages of bulk OC (4,311 ± 2,022 years, $n = 7$). No significant relationship was observed between TOC (Table S1) and the pre-depositional ^{14}C ages of bulk OC over the past *c.* 2,700 years. Since bulk sedimentary OC at this location mainly reflects a mixture of terrestrially sourced pools (e.g., surface and deep soils), we turn to the pre-depositional mean ^{14}C age of LCFAs to understand changes in pre-aged terrestrial matter delivery over the last *c.* 2,700 years (Table S3).

Based on the noted coupling between pre-depositional ^{14}C ages of bulk OC and temperature (Figure 2), we subdivided the pre-depositional mean LCFAs ^{14}C data into pre ($n = 12$) and post ($n = 7$) the end of LIA groups, with a discriminatory threshold at *c.* 100 cal. y BP. The post-LIA samples possessed significantly older LCFAs ^{14}C ages (*t*-test and Wilcoxon test, $p \leq 0.02$) than their older counterparts. A similar conclusion was also reached via application of a balanced Monte Carlo-type bootstrap analysis. Here, LCFAs housed within post-LIA sediments were found to possess significantly older ^{14}C age (929 years) compared with their older counterparts (Figure 4).

4. Discussion

Radiocarbon ages of particulate permafrost OC provide perhaps the best means of tracing changes in permafrost OC release (Wild et al., 2019). For instance, the Kolyma River, within the continuous permafrost zone of eastern Siberia, features particulate OC (POC) with an extremely high pre-aged/modern ratio, signaling the dominance of permafrost OC export throughout its watershed (Wild et al., 2019). For Colville River, the radiocarbon ages of bulk OC from suspended particles collected at the river mouth (6,773 years;

Eglinton et al., 2021) and that from river bed sediments collected in the main channel (10,000 y BP; Zhang et al., 2017) imply mobilization of permafrost via the fluvial system. As stated before, this site is dominated by riverine inputs based on $\delta^{13}C$ and biomarker results compared to other sites in the Colville delta and Simpson Lagoon region (Schreiner et al., 2013; Zhang et al., 2015). The barrier islands shield L1 from intense ice process and make it a depocenter with highest sedimentation rate compared to other sites in the region (Hanna et al., 2014). Deposited at this delta, lateral transport-associated ^{14}C aging of terrestrial OC should be very limited (Bröder et al., 2018). The downcore profile of ^{137}Cs results also imply this site to be a stable deposition environment (Hanna et al., 2014; Lima et al., 2005). The accumulation rate of sediments at this site is relatively stable over the past ~2,700 years according to the age model, except for the uppermost sediments deposited in recent warming period. Thus, the undisturbed sediment record provides an ideal archive from which to decipher changes of permafrost OC exported from the watershed.

Although evidence of permafrost export from Arctic river systems and subsequent coastal deposition in surface sediments has been reported (Feng et al., 2013; Schreiner et al., 2014), our results demonstrate that riverine mobilization of permafrost OC is a long-lived phenomenon that has been occurring at least to some degree for thousands of years. This is consistent with the mobilization of permafrost OC from soil to river and finally to the delta, as indicated by evidence from ^{14}C ramped pyrolysis and lignin biomarkers (Zhang et al., 2017). The close associationof the ^{14}C age of bulk OC with temperature reconstructions from Brooks Range and the Arctic over the past *c.* 1,300 years (Figure 2) likely reveals the modulating role of climate in arctic permafrost dynamics. Dominated by riverine OC inputs, the observed post-LIA increase in pre-depositional ^{14}C age of bulk OC can, in principle, be attributed to either a decreased proportion of young OC or heightened percentage of aged OC. Considering contemporary vegetation expansion (Tape et al., 2006) and relatively higher TOC content in the post-LIA-aged sediments (Figure 3a), diminished fluxes of young and fresh surficial OC inputs are considered unlikely. Therefore, the observed increase in pre-depositional ^{14}C age of bulk OC is more readily attributable to a possible increase of permafrost-derived OC inputs and/or a progressive mobilization of an older, and presumably deeper, OC reservoir. Moreover, since sedimentary LCFAs have been shown to originate mostly from deep permafrost (Feng et al., 2013), the greater pre-depositional mean ^{14}C age of LCFAs in the aftermath of the LIA possibly lends further support to deeper permafrost-derived OC delivery over the last 160 years (Figure 4). These changes are not likely caused by diagenetic process which would be expected to preferentially remove more labile (fresher and younger) OC with increasing diagenesis/depth (Soetaert et al., 1996; Wakeham et al., 1997), contrary to our results showing older ^{14}C ages toward the top of the core. In contrast, post-depositional diagenesis may have dampened the change in the pre-depositional mean ages.

The increase of permafrost-derived OC inputs and/or mobilization of an older and deeper permafrost OC reservoir may stem from several processes, broadly reflecting thermally driven catchment-housed permafrost destabilization. Arctic river systems are highly seasonal, featuring disproportionately high discharge and sediment loads coincident with the spring thaw (Bring et al., 2016; Gordeev, 2006). During this period, ~62% of Colville River's annual sediment load is estimated to transit its catchment, derived, principally, from bank erosion (Walker & Hudson, 2003). The rates of thermal erosion of riverbanks in the Colville main channel and its main tributary (Itkillik River) were averaged to be 0.9 m y^{-1} (Stephani et al., 2019) and 11.4 m y^{-1} (Kanevskiy et al., 2016), respectively. Here, in the absence of insulating vegetation and surface soils (Walker et al., 2003), permafrost exposed within the eroding bluffs is directly exposed to water and warming air (Figure S3). Furthermore, within the eroding riverbanks, top soils are extremely thin compared to the underlying permafrost (Figure S3), thereby bank erosion should enhance the preferential liberation of aged OC, potentially explaining the greater pre-depositional ^{14}C age of bulk OC and LCFAs over the last *c.* 160 years. Apart from bank erosion, widespread degradation of ice wedges, which form thermokarst ponds, has occurred across the Arctic (Jorgenson et al., 2015; Liljedahl et al., 2016). The increase in ice-wedge thermokarst in Alaska is likely related to the exceptionally warm and wet summers observed in 1989 and 1998 (Jorgenson et al., 2015). The intense destabilization of permafrost through thermokarst erosion may also facilitate bank erosion to some extent, providing another potential source of the pre-aged carbon found in post-LIA sediments.

Underlain by continuous permafrost, the lateral transport of OC in the watershed may not show apparent changes. Despite increased temperature in this region, thaw depth to the active layer has apparently

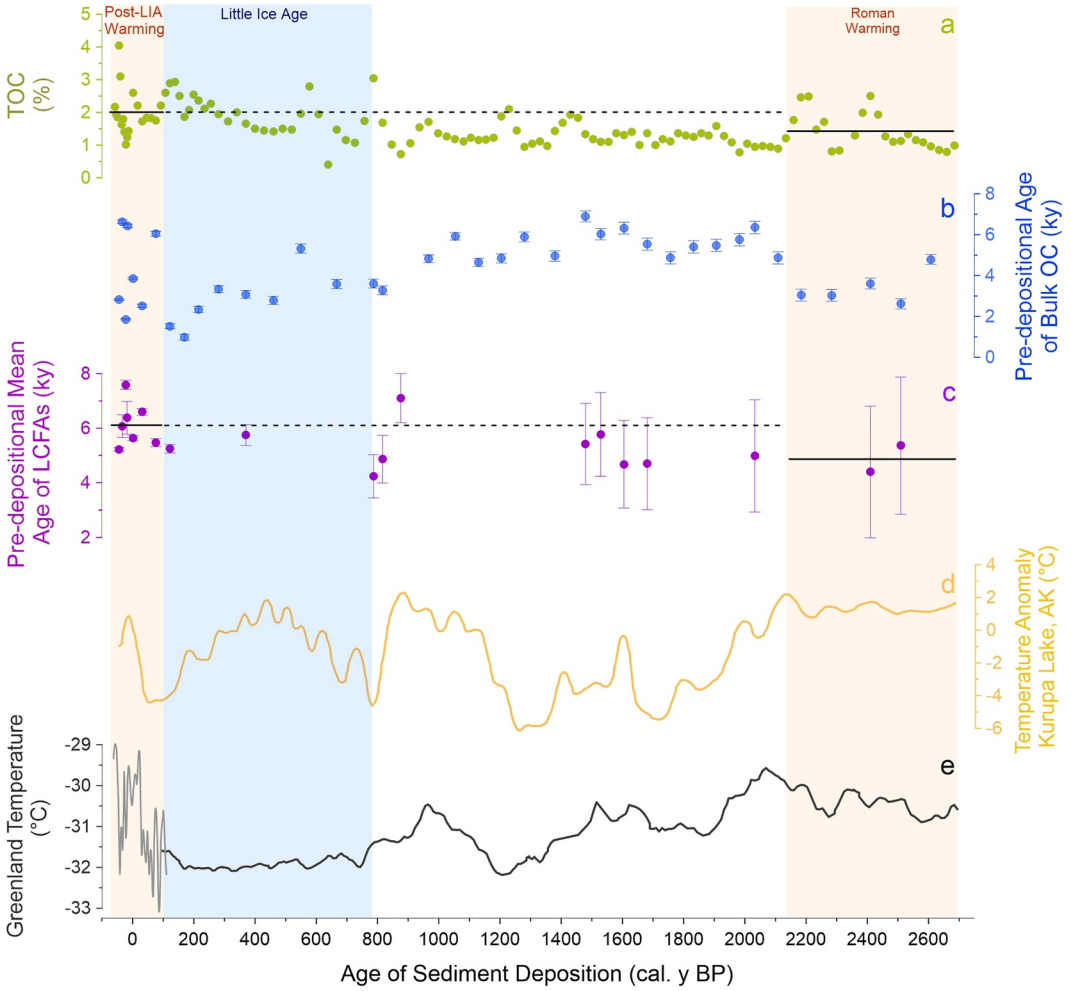

Figure 3. A geochemical and geochronological record of late Holocene permafrost thawing within the Colville River watershed. (a) Total organic carbon (TOC); (b) pre-depositional ^{14}C age of bulk organic carbon; (c) pre-depositional mean ^{14}C age of long-chain fatty acids (LCFAs); (d) summer temperature anomaly for Kurupa Lake in Brooks Range, Alaska (e) GISP2 ice-core-derived (black; Alley, 2004) and LOESS smoothed Greenland temperature record (gray; Cappelen & Vinther, 2014). Pre-depositional ^{14}C ages are plotted using the age depth model illustrated in Figure S1. Orange columns depict respective warming episodes discussed within the text and blue column highlights the Little Ice Age. Black horizontal lines in (a) and (c) demonstrate the mean value of parameters in those two warming episodes.

remained stable (Hollister et al., 2006; Shiklomanov et al., 2012). Precipitation in northern Alaska has more or less remained constant over the same period (Bieniek et al., 2014; McAfee et al., 2013). In addition, the low permeability of the frozen soils will have largely curtailed water flow and storage (Bring et al., 2016), indicating limited changes on the export of OC by lateral transport. Even if there was some extent of increase of OC from the upper soils, most likely in the summer, the extremely low water discharge (Holmes et al., 2008) may not be able to deliver most of the upper soil OC to the delta.

Brooks Range and Greenland temperature reconstructions (Boldt, 2015; Cappelen & Vinther, 2014; McKay & Kaufman, 2014) reveal prior intervals of warming, yet these warming intervals show different characteristics when compared to the post-LIA warming episode (Figure 3). For example, during the Roman warming interval (*c.* 2,700–2,100 cal. y BP), TOC ($n = 22$) was significantly lower than that seen during the post-LIA ($n = 18$) warming episode (*t*-test, $p < 0.01$), yet the pre-depositional ^{14}C ages of bulk OC are not significantly different from the post-LIA (Figure 3). While only two pre-depositional mean ^{14}C ages of LCFAs are available from Roman warming period, they are younger (4,880 ± 681 y BP, $n = 2$) than those from the post-LIA warming era (6,138 ± 810 y, $n = 7$), potentially signaling a less pronounced release of pre-aged carbon. We speculate that the generally cooler prevailing temperatures at the beginning of the post-LIA warming

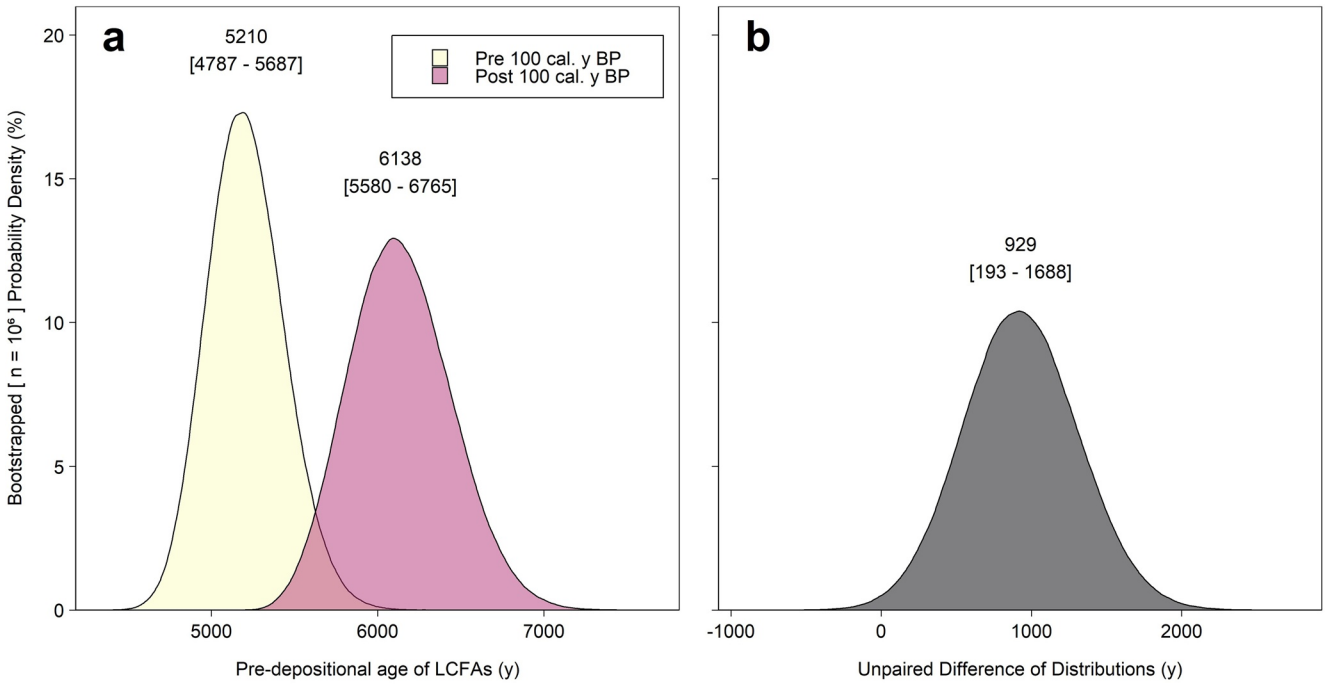

Figure 4. Bootstrap-generated ^{14}C age probability density distributions derived from pre-depositional mean long-chain fatty acids (LCFAs) ages in periods pre (>100 cal. y BP) and post (<100 cal. y BP) (a) the end of Little Ice Age and (b) their difference after subtraction. Mean ages and parenthesized 95% confidence intervals accompany each distribution.

episode compared with those for the Roman warming trend (6°C and 1°C cooler in Brooks Range and Greenland, respectively; Figures 3d and 3e), coupled with a more rapid temperature increase (551 and 12 times faster in Brooks Rang and Greenland, respectively; Figures 3d and 3e), may have played an important role in modulating permafrost dynamics and/or the balance between vegetation-induced carbon burial and thermally driven permafrost losses. Furthermore, mobilization of permafrost OC may have also been greater during the post-LIA warming because of preceding glacier expansion, and the corresponding growth of fresh-water stocks during the LIA (Solomina et al., 2016; Wanner et al., 2008). Accelerated warming may have triggered extensive glacial melting (Chen et al., 2006; Vargo et al., 2020), which would enhance infiltration and bank erosion, inducing more OC mobilization throughout the watershed. Rising Arctic temperatures should also increase plant carbon uptake (Elmendorf et al., 2012; Pearson et al., 2013), offering a negative feedback to offset the carbon losses from permafrost thawing. This effect, however, may be more important during a more modest warming regime, where the ecosystem would have more time to adapt to the climate perturbation (Gałka et al., 2018). Clearly the involvement and significance of these competing mechanisms requires thorough exploration; however, for now, it is clear that permafrost destruction cannot be linearly extrapolated from temperature reconstructions.

Mechanistic uncertainties notwithstanding, the observed increase in the ^{14}C ages of bulk OC and LCFAs archived in post-LIA sediments deposited in the Colville River delta indicates an increased thawing and mobilization of permafrost OC over the last *c*.160 years. This increase in ^{14}C age occurs in concert with a positive inflection in temperature reconstructions from Simpson Lagoon (Hanna et al., 2018), lakes within the Brooks Range (Bird et al., 2009; Boldt et al., 2015), and the wider Arctic region (Alley, 2004; Cappelen & Vinther, 2014; McKay & Kaufman, 2014). Permafrost thawing has recently been linked to CO_2-driven temperature fluctuations operating over glacial-interglacial transitions (Crichton et al., 2016). Our results, therefore, lend support to the notion that such fluctuations can influence permafrost dynamics at sub-centennial timescales. Moreover, our down-core study provides relatively reliable evidence linking permafrost thawing and the export of pre-aged terrestrial OC via Arctic river systems, serving as a baseline for future pan-Arctic comparisons. The contrast between Roman and post-LIA warming trends imply that the rate of warming and the prevailing boundary conditions are important modulators of permafrost thawing;

however, more work is clearly needed to refine these suppositions. Accordingly, the application of ^{14}C analysis of bulk OC and source-diagnostic compounds to long-term sediment records from other Arctic coastal regions remains a priority. In particular, the geological record offers unparalleled insights into how past changes in the magnitude and pace of warming and associated changes in boundary conditions (e.g., prevailing temperature, and glacial structure/dynamics) may influence the fate of the Arctic's permafrost reserves. Understanding of permafrost-driven climate feedbacks remains a fundamental prerequisite for accurate climate simulations.

Conflict of Interest

The authors declare no conflicts of interest relevant to this study.

Data Availability Statement

The data needed to evaluate the manuscript's conclusions are currently provided in supplementary tables and are available for public access in Open Science Framework repository.

Acknowledgments
This research was supported by the National Science Foundation (NSF; ARC-0935336, OPP-80937700 and ARC-1023623), a NOSAMS initiative research grant and the Jon and Beverly Thompson Endowed Chair of Geological Sciences (UF). X. Zhang and G. Izon acknowledge support from the Simons Collaboration on the Origins of Life during the drafting stage of this manuscript. Members of the Laboratory of Ion Beam Physics (ETH Zurich) are thanked for their AMS support.

References

Alley, R. B. (2004). GISP2 ice core temperature and accumulation data. *IGBP PAGES/World Data Center for Paleoclimatology Data Contribution Series, 13*.

Baskaran, M., Bianchi, T. S., & Filley, T. R. (2017). Inconsistencies between ^{14}C and short-lived radionuclides-based sediment accumulation rates: Effects of long-term remineralization. *Journal of Environmental Radioactivity*, *174*, 10–16. https://doi.org/10.1016/j.jenvrad.2016.07.028

Bianchi, T. S., & Allison, M. A. (2009). Large-river delta-front estuaries as natural "recorders" of global environmental change. *Proceedings of the National Academy of Sciences of the United States of America*, *106*, 8085–8092. https://doi.org/10.1073/pnas.0812878106

Bianchi, T. S., & Canuel, E. A. (2011). *Chemical biomarkers in aquatic ecosystems*. Princeton University Press.

Bieniek, P. A., Walsh, J. E., Thoman, R. L., & Bhatt, U. S. (2014). Using climate divisions to analyze variations and trends in Alaska temperature and precipitation. *Journal of Climate*, *27*(8), 2800–2818. https://doi.org/10.1175/jcli-d-13-00342.1

Bird, B. W., Abbott, M. B., Finney, B. P., & Kutchko, B. (2009). A 2000 year varve-based climate record from the central Brooks Range, Alaska. *Journal of Paleolimnology*, *41*(1), 25–41. https://doi.org/10.1007/s10933-008-9262-y

Blaauw, M., & Christen, J. A. (2011). Flexible paleoclimate age-depth models using an autoregressive gamma process. *Bayesian Analysis*, *6*(3), 457–474. https://doi.org/10.1214/ba/1339616472

Boldt, B. R., Kaufman, D. S., McKay, N. P., & Briner, J. P. (2015). Holocene summer temperature reconstruction from sedimentary chlorophyll content, with treatment of age uncertainties, Kurupa Lake, Arctic Alaska. *The Holocene*, *25*(4), 641–650. https://doi.org/10.1177/0959683614565929

Bring, A., Fedorova, I., Dibike, Y., Hinzman, L., Mård, J., Mernild, S. H., et al. (2016). Arctic terrestrial hydrology: A synthesis of processes, regional effects, and research challenges. *Journal of Geophysical Research: Biogeosciences*, *121*(3), 621–649. https://doi.org/10.1002/2015jg003131

Bröder, L., Tesi, T., Andersson, A., Semiletov, I., & Gustafsson, Ö. (2018). Bounding cross-shelf transport time and degradation in Siberian-Arctic land-ocean carbon transfer. *Nature Communications*, *9*(1), 1–8.

Brown, J., Ferrians, O., Jr, Heginbottom, J., & Melnikov, E. (1997). *Circum-Arctic map of permafrost and ground-ice conditions*. Reston, VA: US Geological Survey.

Cappelen, J., & Vinther, B. M. (2014). *SW Greenland temperature data 1784-2013*, (Technical Report 14-06).

Chen, J. L., Tapley, B. D., & Wilson, C. R. (2006). Alaskan mountain glacial melting observed by satellite gravimetry. *Earth and Planetary Science Letters*, *248*(1–2), 368–378. https://doi.org/10.1016/j.epsl.2006.05.039

Crichton, K. A., Bouttes, N., Roche, D. M., Chappellaz, J., & Krinner, G. (2016). Permafrost carbon as a missing link to explain CO_2 changes during the last deglaciation. *Nature Geoscience*, *9*(9), 683–686. https://doi.org/10.1038/ngeo2793

Davies, L. J., Appleby, P., Jensen, B. J. L., Magnan, G., Mullan-Boudreau, G., Noernberg, T., et al. (2018). High-resolution age modelling of peat bogs from northern Alberta, Canada, using pre- and post-bomb ^{14}C, ^{210}Pb and historical cryptotephra. *Quaternary Geochronology*, *47*, 138–162. https://doi.org/10.1016/j.quageo.2018.04.008

Dunton, K. H., Weingartner, T., & Carmack, E. C. (2006). The nearshore western Beaufort Sea ecosystem: Circulation and importance of terrestrial carbon in arctic coastal food webs. *Progress in Oceanography*, *71*(2–4), 362–378. https://doi.org/10.1016/j.pocean.2006.09.011

Eglinton, T. I., Aluwihare, L. I., Bauer, J. E., Druffel, E. R. M., & McNichol, A. P. (1996). Gas chromatographic isolation of individual compounds from complex matrices for radiocarbon dating. *Analytical Chemistry*, *68*(5), 904–912. https://doi.org/10.1021/ac9508513

Eglinton, T. I., Galy, V. V., Hemingway, J. D., Feng, X., Bao, H., Blattmann, T. M., et al. (2021). Climate control on terrestrial biospheric carbon turnover. *Proceedings of the National Academy of Sciences of the United States of America*, *118*, e2011585118.

Elmendorf, S. C., Henry, G. H. R., Hollister, R. D., Björk, R. G., Boulanger-Lapointe, N., Cooper, E. J., et al. (2012). Plot-scale evidence of tundra vegetation change and links to recent summer warming. *Nature Climate Change*, *2*(6), 453–457. https://doi.org/10.1038/nclimate1465

Feng, X., Gustafsson, Ö., Holmes, R. M., Vonk, J. E., van Dongen, B. E., Semiletov, I. P., et al. (2015). Multimolecular tracers of terrestrial carbon transfer across the pan-Arctic: ^{14}C characteristics of sedimentary carbon components and their environmental controls. *Global Biogeochemical Cycles*, *29*(11), 1855–1873. https://doi.org/10.1002/2015gb005204

Feng, X., Vonk, J. E., Van Dongen, B. E., Gustafsson, O., Semiletov, I. P., Dudarev, O. V., et al. (2013). Differential mobilization of terrestrial carbon pools in Eurasian Arctic river basins. *Proceedings of the National Academy of Sciences of the United States of America*, *110*, (14168–14173). https://doi.org/10.1073/pnas.1307031110

Gałka, M., Swindles, G. T., Szal, M., Fulweber, R., & Feurdean, A. (2018). Response of plant communities to climate change during the late Holocene: Palaeoecological insights from peatlands in the Alaskan Arctic. *Ecological Indicators*, *85*, 525–536.

Gordeev, V. (2006). Fluvial sediment flux to the Arctic Ocean. *Geomorphology*, *80*(1–2), 94–104. https://doi.org/10.1016/j.geomorph.2005.09.008

Haghipour, N., Ausín, B., Usman, M. O., Ishikawa, N., Wacker, L., Welte, C., et al. (2018). Compound-specific radiocarbon analysis by Elemental Analyzer-Accelerator Mass Spectrometry: Precision and limitations. *Analytical Chemistry*, *91*(3), 2042–2049. https://doi.org/10.1021/acs.analchem.8b04491

Hanna, A. J., Allison, M. A., Bianchi, T. S., Marcantonio, F., & Goff, J. A. (2014). Late Holocene sedimentation in a high Arctic coastal setting: Simpson Lagoon and Colville Delta, Alaska. *Continental Shelf Research*, *74*, 11–24. https://doi.org/10.1016/j.csr.2013.11.026

Hanna, A. J., Shanahan, T. M., Allison, M. A., Bianchi, T. S., & Schreiner, K. M. (2018). A multi-proxy investigation of late-Holocene temperature change and climate-driven fluctuations in sediment sourcing: Simpson Lagoon, Alaska. *The Holocene*, *28*(6), 984–997. https://doi.org/10.1177/0959683617752845

Harris, D., Horwáth, W. R., & Van Kessel, C. (2001). Acid fumigation of soils to remove carbonates prior to total organic carbon or carbon-13 isotopic analysis. *Soil Science Society of America Journal*, *65*(6), 1853–1856. https://doi.org/10.2136/sssaj2001.1853

Hinzman, L. D., Bettez, N. D., Bolton, W. R., Chapin, F. S., Dyurgerov, M. B., Fastie, C. L., et al. (2005). Evidence and implications of recent climate change in northern Alaska and other arctic regions. *Climatic Change*, *72*(3), 251–298. https://doi.org/10.1007/s10584-005-5352-2

Hollister, R. D., Webber, P. J., Nelson, F. E., & Tweedie, C. E. (2006). Soil thaw and temperature response to air warming varies by plant community: Results from an open-top chamber experiment in northern Alaska. *Arctic Antarctic and Alpine Research*, *38*(2), 206–215. https://doi.org/10.1657/1523-0430(2006)38[206:statrt]2.0.co;2

Holmes, R. M., McClelland, J. W., Raymond, P. A., Frazer, B. B., Peterson, B. J., & Stieglitz, M. (2008). Lability of DOC transported by Alaskan rivers to the Arctic Ocean. *Geophysical Research Letters*, *35*, L03402. https://doi.org/10.1029/2007gl032837

Jorgenson, M. T., Kanevskiy, M., Shur, Y., Moskalenko, N., Brown, D. R. N., Wickland, K., et al. (2015). Role of ground ice dynamics and ecological feedbacks in recent ice wedge degradation and stabilization. *Journal of Geophysical Research: Earth Surfaces*, *120*(11), 2280–2297. https://doi.org/10.1002/2015jf003602

Kanevskiy, M., Shur, Y., Strauss, J., Jorgenson, T., Fortier, D., Stephani, E., & Vasiliev, A. (2016). Patterns and rates of riverbank erosion involving ice-rich permafrost (yedoma) in northern Alaska. *Geomorphology*, *253*, 370–384. https://doi.org/10.1016/j.geomorph.2015.10.023

Koven, C. D., Ringeval, B., Friedlingstein, P., Ciais, P., Cadule, P., Khvorostyanov, D., et al. (2011). Permafrost carbon-climate feedbacks accelerate global warming. *Proceedings of the National Academy of Sciences of the United States of America*, *108*, 14769–14774. https://doi.org/10.1073/pnas.1103910108

Liljedahl, A. K., Boike, J., Daanen, R. P., Fedorov, A. N., Frost, G. V., Grosse, G., et al. (2016). Pan-Arctic ice-wedge degradation in warming permafrost and its influence on tundra hydrology. *Nature Geoscience*, *9*(4), 312–318. https://doi.org/10.1038/ngeo2674

Lima, A. L., Hubeny, J. B., Reddy, C. M., King, J. W., Hughen, K. A., & Eglinton, T. I. (2005). High-resolution historical records from Pettaquamscutt River basin sediments: 1. ^{210}Pb and varve chronologies validate record of ^{137}Cs released by the Chernobyl accident. *Geochimica et Cosmochimica Acta*, *69*(7), 1803–1812. https://doi.org/10.1016/j.gca.2004.10.009

McAfee, S. A., Guentchev, G., & Eischeid, J. K. (2013). Reconciling precipitation trends in Alaska: 1. Station-based analyses. *Journal of Geophysical Research: Atmospheres*, *118*(14), 7523–7541. https://doi.org/10.1002/jgrd.50572

McGuire, A. D., Anderson, L. G., Christensen, T. R., Dallimore, S., Guo, L., Hayes, D. J., et al. (2009). Sensitivity of the carbon cycle in the Arctic to climate change. *Ecological Monographs*, *79*(4), 523–555. https://doi.org/10.1890/08-2025.1

McKay, N. P., & Kaufman, D. S. (2014). An extended Arctic proxy temperature database for the past 2,000 years. *Scientific Data*, *1*, 140026.

Michaelson, G., & Ping, C. (2003). Soil organic carbon and CO_2 respiration at subzero temperature in soils of Arctic Alaska. *Journal of Geophysical Research*, *108*(D2), 5-1–5-10. https://doi.org/10.1029/2001jd000920

Miller, A. J., & Kuehl, S. A. (2010). Shelf sedimentation on a tectonically active margin: A modern sediment budget for Poverty continental shelf, New Zealand. *Marine Geology*, *270*(1–4), 175–187. https://doi.org/10.1016/j.margeo.2009.10.018

Pearson, R. G., Phillips, S. J., Loranty, M. M., Beck, P. S. A., Damoulas, T., Knight, S. J., & Goetz, S. J. (2013). Shifts in Arctic vegetation and associated feedbacks under climate change. *Nature Climate Change*, *3*(7), 673–677. https://doi.org/10.1038/nclimate1858

Raynolds, M. K., Walker, D. A., Ambrosius, K. J., Brown, J., Everett, K. R., Kanevskiy, M., et al. (2014). Cumulative geoecological effects of 62 years of infrastructure and climate change in ice-rich permafrost landscapes, Prudhoe Bay Oilfield, Alaska. *Global Change Biology*, *20*(4), 1211–1224. https://doi.org/10.1111/gcb.12500

Rosenheim, B. E., & Galy, V. (2012). Direct measurement of riverine particulate organic carbon age structure. *Geophysical Research Letters*, *39*, L19703. https://doi.org/10.1029/2012gl052883

Schädel, C., Bader, M. K.-F., Schuur, E. A. G., Biasi, C., Bracho, R., Čapek, P., et al. (2016). Potential carbon emissions dominated by carbon dioxide from thawed permafrost soils. *Nature Climate Change*, *6*(10), 950–953. https://doi.org/10.1038/nclimate3054

Schreiner, K. M., Bianchi, T. S., Eglinton, T. I., Allison, M. A., & Hanna, A. J. M. (2013). Sources of terrigenous inputs to surface sediments of the Colville River Delta and Simpson's Lagoon, Beaufort Sea, Alaska. *Journal of Geophysical Research: Biogeosciences*, *118*(2), 808–824. https://doi.org/10.1002/jgrg.20065

Schreiner, K. M., Bianchi, T. S., & Rosenheim, B. E. (2014). Evidence for permafrost thaw and transport from an Alaskan North Slope watershed. *Geophysical Research Letters*, *41*(9), 3117–3126. https://doi.org/10.1002/2014gl059514

Schumacher, B. A. (2002). *Methods for the determination of total organic carbon (TOC) in soils and sediments*. U.S. Environmental Protection Agency.

Schuur, E. A. G., Bockheim, J., Canadell, J. G., Euskirchen, E., Field, C. B., Goryachkin, S. V., et al. (2008). Vulnerability of permafrost carbon to climate change: Implications for the global carbon cycle. *BioScience*, *58*(8), 701–714. https://doi.org/10.1641/b580807

Schuur, E. A. G., McGuire, A. D., Schädel, C., Grosse, G., Harden, J. W., Hayes, D. J., et al. (2015). Climate change and the permafrost carbon feedback. *Nature*, *520*(7546), 171–179. https://doi.org/10.1038/nature14338

Shiklomanov, N. I., Streletskiy, D. A., & Nelson, F. E. (2012). *Northern hemisphere component of the global circumpolar active layer monitoring (CALM) program*. Paper presented at the Proceedings of the 10th International Conference on Permafrost.

Smith, L. C., Sheng, Y., MacDonald, G., & Hinzman, L. (2005). Disappearing arctic lakes. *Science*, *308*(5727), 14291429. https://doi.org/10.1126/science.1108142

Soetaert, K., Herman, P. M. J., & Middelburg, J. J. (1996). A model of early diagenetic processes from the shelf to abyssal depths. *Geochimica et Cosmochimica Acta*, *60*(6), 1019–1040. https://doi.org/10.1016/0016-7037(96)00013-0

Solomina, O. N., Bradley, R. S., Jomelli, V., Geirsdottir, A., Kaufman, D. S., Koch, J., et al. (2016). Glacier fluctuations during the past 2000 years. *Quaternary Science Reviews*, *149*, 61–90. https://doi.org/10.1016/j.quascirev.2016.04.008

Stephani, E., Jones, B., & Kanevskiy, M. (2019). Assessing riverbank erosion and land cover changes in permafrost regions based on a terrain analysis approach: An example from the Colville River Delta, Northern Alaska. In *Cold Regions Engineering 2019* (pp. 678–686). Reston, VA: American Society of Civil Engineers.

Tape, K., Sturm, M., & Racine, C. (2006). The evidence for shrub expansion in Northern Alaska and the Pan-Arctic. *Global Change Biology*, *12*(4), 686–702. https://doi.org/10.1111/j.1365-2486.2006.01128.x

Tesi, T., Muschitiello, F., Smittenberg, R. H., Jakobsson, M., Vonk, J., Hill, P., et al. (2016). Massive remobilization of permafrost carbon during post-glacial warming. *Nature Communications*, *7*, 13653.

Vargo, L. J., Anderson, B. M., Dadić, R., Horgan, H. J., Mackintosh, A. N., King, A. D., & Lorrey, A. M. (2020). Anthropogenic warming forces extreme annual glacier mass loss. *Nature Climate Change*, *10*(9), 856–861. https://doi.org/10.1038/s41558-020-0849-2

Venkatesan, M. I., Naidu, A. S., Blanchard, A. L., Misra, D., & Kelley, J. J. (2013). Historical changes in trace metals and hydrocarbons in nearshore sediments, Alaskan Beaufort Sea, prior and subsequent to petroleum-related industrial development: Part II. Hydrocarbons. *Marine Pollution Bulletin*, *77*(1–2), 147–164. https://doi.org/10.1016/j.marpolbul.2013.10.012

Vetter, L., Rosenheim, B. E., Fernandez, A., & Törnqvist, T. E. (2017). Short organic carbon turnover time and narrow ^{14}C age spectra in early Holocene wetland paleosols. *Geochemistry, Geophysics, Geosystems*, *18*(1), 142–155. https://doi.org/10.1002/2016gc006526

Vonk, J. E., Sánchez-García, L., Van Dongen, B. E., Alling, V., Kosmach, D., Charkin, A., et al. (2012). Activation of old carbon by erosion of coastal and subsea permafrost in Arctic Siberia. *Nature*, *489*(7414), 137–140. https://doi.org/10.1038/nature11392

Wakeham, S. G., Hedges, J. I., Lee, C., Peterson, M. L., & Hernes, P. J. (1997). Compositions and transport of lipid biomarkers through the water column and surficial sediments of the equatorial Pacific Ocean. *Deep Sea Research Part II: Topical Studies in Oceanography*, *44*(9–10), 2131–2162. https://doi.org/10.1016/s0967-0645(97)00035-0

Walker, D. A., Jia, G. J., Epstein, H. E., Raynolds, M. K., Chapin, F. S., III, Copass, C., et al. (2003). Vegetation-soil-thaw-depth relationships along a low-arctic bioclimate gradient, Alaska: Synthesis of information from the ATLAS studies. *Permafrost and Periglacial Processes*, *14*(2), 103–123. https://doi.org/10.1002/ppp.452

Walker, D. A., Raynolds, M. K., Daniëls, F. J. A., Einarsson, E., Elvebakk, A., Gould, W. A., et al. (2005). The circumpolar Arctic vegetation map. *Journal of Vegetation Science*, *16*(3), 267–282. https://doi.org/10.1111/j.1654-1103.2005.tb02365.x

Walker, H. J., & Hudson, P. F. (2003). Hydrologic and geomorphic processes in the Colville River delta, Alaska. *Geomorphology*, *56*(3–4), 291–303. https://doi.org/10.1016/s0169-555x(03)00157-0

Wanner, H., Beer, J., Bütikofer, J., Crowley, T. J., Cubasch, U., Flückiger, J., et al. (2008). Mid-to Late Holocene climate change: An overview. *Quaternary Science Reviews*, *27*(19–20), 1791–1828. https://doi.org/10.1016/j.quascirev.2008.06.013

Wild, B., Andersson, A., Bröder, L., Vonk, J., Hugelius, G., McClelland, J. W., et al. (2019). Rivers across the Siberian Arctic unearth the patterns of carbon release from thawing permafrost. *Proceedings of the National Academy of Sciences of the United States of America*, *116*(21), 10280–10285. https://doi.org/10.1073/pnas.1811797116

Winterfeld, M., Mollenhauer, G., Dummann, W., Köhler, P., Lembke-Jene, L., Meyer, V. D., et al. (2018). Deglacial mobilization of pre-aged terrestrial carbon from degrading permafrost. *Nature Communications*, *9*(1), 3666.

Xu, X., Trumbore, S. E., Zheng, S., Southon, J. R., McDuffee, K. E., Luttgen, M., & Liu, J. C. (2007). Modifying a sealed tube zinc reduction method for preparation of AMS graphite targets: Reducing background and attaining high precision. *Nuclear Instruments and Methods in Physics Research Section B: Beam Interactions with Materials and Atoms*, *259*(1), 320–329. https://doi.org/10.1016/j.nimb.2007.01.175

Zhang, X., Bianchi, T. S., & Allison, M.A. (2015). Sources of organic matter in sediments of the Colville River delta, Alaska: A multi-proxy approach. *Organic Geochemistry*, *87*, 96–106.

Zhang, X., Bianchi, T. S., Cui, X., Rosenheim, B. E., Ping, C. L., Hanna, A. J., et al. (2017). Permafrost organic carbon mobilization from the watershed to the Colville River Delta: Evidence from ^{14}C ramped pyrolysis and lignin biomarkers. *Geophysical Research Letters*, *44*(22), 11491–11500. https://doi.org/10.1002/2017gl075543